

# Quantum Support Vector Machines for Continuum Suppression in B Meson Decays

Jamie Heredge · Charles Hill · Lloyd Hollenberg · Martin Seviar

Received: date / Accepted: date

**Abstract** Quantum computers have the potential for speed-ups of certain computational tasks. A possibility this opens up within the field of machine learning is the use of quantum features that would be inefficient to calculate classically. Machine learning algorithms are ubiquitous in particle physics and as advances are made in quantum machine learning technology, there may be a similar adoption of these quantum techniques. In this work a quantum support vector machine (QSVM) is implemented for signal-background classification. We investigate the effect of different quantum encoding circuits, the process that transforms classical data into a quantum state, on the final classification performance. We show an encoding approach that achieves an Area Under Receiver Operating Characteristic Curve (AUC) of 0.877 determined using quantum circuit simulations. For this same dataset the best classical method, a classical Support Vector Machine (SVM) using the Radial Basis Function (RBF) Kernel achieved an AUC of 0.865. Using a reduced dataset we then ran the algorithm on the IBM Quantum *ibmq\_casablanca* device achieving an average AUC of 0.703. As further improvements to the error rates and availability of quantum computers materialise, they could form a new approach for data analysis in high energy physics.

**Keywords** Quantum Machine Learning · Quantum Support Vector Machines · Particle Physics · Continuum Suppression · Belle II

## 1 Introduction

There are a number of measurements in flavour physics that are statistically limited due to lack of precision in signal-background classification. A superior classification algorithm would allow improved measurements and may result in the discovery of physics beyond the standard model. With the emergence of programmable quantum computer devices, we design and implement a quantum support vector machine approach for the signal-background classification task in B meson decays. In a B meson factory an electron and positron are collided, in our dataset this results in the creation of either (1) a pair of B and anti-B mesons decayed from the  $\Upsilon(4S)$ , or (2) a lighter quark and anti-quark  $q\bar{q}$  pair. The B-mesons will quickly decay and the  $q\bar{q}$  will hadronise into an array of other longer-lived particles which are measured by the Belle II detector. To investigate a specific B meson decay mode, such as  $B \rightarrow K^+K^-$  in our dataset, we select only events that contain particle tracks identified as  $K^+K^-$  that could have originated from B mesons (which will include some falsely identified  $K^+K^-$  tracks from the quark / anti-quark pair) we refer to these particles as from the B candidate. Given the momentum data of all the other final particles in the event, the task is to classify between the two initial situations. The B meson / anti-B meson pair event is referred to as a signal event; the quark / anti-quark pair event is referred to as a continuum background event and these comprise the primary background for many studies of B-meson decays, many of which have branch-

Jamie Heredge, Charles Hill, Lloyd Hollenberg, Martin Seviar  
School of Physics, University of Melbourne, Parkville, VIC,  
3020, Australia

E-mail: jamie.heredge@student.unimelb.edu.au

E-mail: cdhill@unimelb.edu.au

E-mail: lloydch@unimelb.edu.au

E-mail: martines@unimelb.edu.au

Charles Hill

School of Mathematics and Statistics, University of Melbourne,  
Parkville, VIC, 3010, Australia

E-mail: cdhill@unimelb.edu.au

ing ratios smaller than  $10^{-5}$ . It is therefore important to suppress the presence of continuum background events in the data. A better classification algorithm between signal and background events enables improved precision in measurements of these rare B-meson decays.

Quantum computer hardware is advancing rapidly. Quantum supremacy has been achieved [3] by demonstrating a calculation on a quantum machine that outperformed classical high performance computers. More recently a photonic quantum system achieved a sampling rate of order  $10^{14}$  above state-of-the-art simulations and supercomputers, completing a task that would be estimated to take current supercomputers several billions of years [28]. As the size and quality of quantum computers continues to advance, with large-scale entanglement achieved in a range of platforms [17], so does the feasibility of using quantum machines to perform classification tasks in particle physics. In particular, there are various ways in which the field of machine learning may benefit from the advent of quantum computing. These benefits range from speed-ups to specific subroutines, such as gradient descent [21], to quantum analogues of classical algorithms, for example quantum neural networks [12]. We focus on the quantum analogue of the support vector machine that is proposed by Havlicek et al [10], specifically the kernel estimation technique. This QSVM approach involves using a quantum circuit to estimate the inner product between two datapoints that have been encoded into a higher dimensional quantum Hilbert space. This forms a kernel matrix which is then passed to a classical support vector machine. QSVM approaches have been found to outperform classical SVMs on various machine learning benchmark datasets [19] and techniques involving preprocessing for QSVM approaches have led to improved performance on Character Recognition datasets [27].

It has been suggested that variational quantum machine learning models can be fundamentally formulated as quantum kernel methods [22]. The global minimum of the cost function for a given quantum model is therefore defined by the kernel and thus the data encoding strategy. This highlights the importance of the data encoding step in any quantum model. Techniques such as quantum metric learning have demonstrated trainable data encoding strategies that aim to maximise distance between separate classes in the higher dimensional Hilbert space [16]. In this paper we explore various data encoding methods that aim to capture the underlying structure of the data while also being easy to implement on current quantum machines.

Machine learning is widely employed in High Energy Physics [2]. Classically the signal-background classification task has been tackled with the use of constructed

variables. This involves creating metrics from the momentum data, such as Fox-Wolfram moments, which are then used as inputs to a classical machine learning algorithm e.g. a boosted decision tree [13,15]. Our focus is on using the raw momentum data as the input to a quantum algorithm. This quantum algorithm then generates a kernel matrix that can be passed to a classical algorithm (a Support Vector Machine) to perform the classification. This approach allows us to test whether quantum circuits are capable of generating useful novel encodings for this classification problem.

The use of variational quantum machine learning techniques have shown that discrimination of interesting events from background is feasible [25,26]. Alternative applications of quantum algorithms within particle physics have also included particle track reconstruction, utilising both quantum annealers [4] and quantum neural networks [5]. A review of quantum machine learning in particle physics was carried out by Guan et al [9].

## 2 Problem Statement

Excluding the particles from the B candidate, our final dataset consists of  $p$  particles with known momentum and therefore  $3p$  inputs corresponding to the 3 momentum components of each particle. Our aim is to produce an algorithm that takes particle momenta as an input and outputs a classification score of 0 for background events and 1 for signal events. The two performance metrics we report are the accuracy (percentage of correct classifications from all predictions) and the Area Under Receiver Operating Characteristic Curve (AUC).

## 3 Implementation

This method focuses on encoding raw momentum data into a quantum state using a quantum circuit. In order to use the raw data in this way, each event is subject to the preprocessing steps illustrated in Figure 1. We first boost our coordinates to the centre of momentum frame of the event. We then rotate the event such that  $\theta = 0$  and  $\theta = \pi$  are aligned with the thrust axis of the event. The thrust axis  $\hat{\mathbf{n}}$  is calculated by maximizing  $T(\hat{\mathbf{n}})$ , defined as

$$T(\hat{\mathbf{n}}) = \frac{\sum_i |\mathbf{P}_i \cdot \hat{\mathbf{n}}|}{\sum_i |\mathbf{P}_i|}. \quad (1)$$

Where  $\mathbf{P}_i$  is a momentum vector belonging to the  $i$ th particle from either the  $B$  candidate or all of the other particles in the event (excluding the  $B$  candidate) [8]. The momentum of a particle in this frame is represented

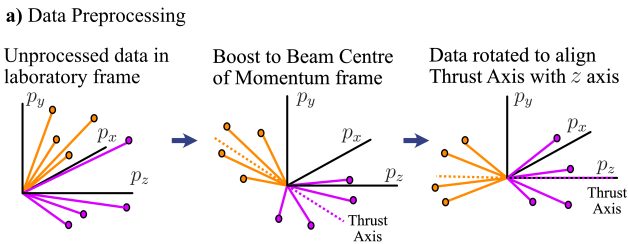


**Fig. 1** An illustration of the preprocessing steps performed on an example quark / anti-quark event.

by three variables in spherical coordinates  $(p, \theta, \phi)$  where  $p$  is the absolute value of the momentum,  $\theta$  is the angle between the particle and the thrust axis and  $\phi$  the angle about the thrust axis.

In the centre of mass frame the  $e^+e^- \rightarrow q\bar{q}$  pair are formed with substantially more individual momentum than the  $e^+e^- \rightarrow \mathcal{T}(4S) \rightarrow B\bar{B}$  pair. Thus the overall distribution of background final state particles are far more "jet-like" than the "spherically" distributed signal particles. Machine learning algorithms can be trained to distinguish these differences.

Quantum rotation gates accept inputs in the range  $[0, 2\pi]$ . The  $\theta$  and  $\phi$  inputs fall naturally into this range. The absolute momentum value  $p$  for our data is normalised by a factor  $\frac{\pi}{p_{max}}$ , where  $p_{max}$  is the highest momentum value found in the entire dataset, in order for the absolute momentum to take a value between  $[0, \pi]$ . This ensures the momentum values of 0 and  $p_{max}$  are maximally separated. After preprocessing the data it is then possible to classify the data using a Quantum Support Vector Machine model [10].

### 3.1 Quantum Support Vector Machine

A classical Support Vector Machine usually works by constructing a hyperplane to separate datapoints that are encoded into a higher dimensional space [20, 23]. In this construction it aims to maximise the distance between the hyperplane and the nearest datapoint of any class. Given  $N$  training vectors  $\mathbf{x}_i$  each with one of two class labels denoted by  $y_i \in 1, -1$ , this construction can be achieved by optimising the following

$$\min_{\alpha} \frac{1}{2} \alpha^T Q \alpha - e^T \alpha; \text{subject to } y^T \alpha = 0. \quad (2)$$

Where  $e$  is a vector with all elements equal to one.  $Q$  is an  $N$  by  $N$  positive semidefinite matrix  $Q_{ij} = y_i y_j K(\mathbf{x}_i, \mathbf{x}_j)$  [24]. The term  $K(\mathbf{x}_i, \mathbf{x}_j) = \phi(\mathbf{x}_i)^T \phi(\mathbf{x}_j)$  is referred to as the kernel matrix. Each datapoint is transformed into a higher dimension by the encoding  $\mathbf{x}_j \rightarrow \phi(\mathbf{x}_j)$ . The explicit form of this encoding is not

required by the Support Vector Machine, which only needs to know the kernel matrix that is usually given as an explicit function.

For the Quantum Support Vector Machine [10] the higher dimensional encoding  $\mathbf{x}_j \rightarrow |\psi(\mathbf{x}_j)\rangle$  is a quantum state which can not be read by a classical algorithm. However, as only the inner product between these quantum encoded states is required it is possible to measure  $|\langle \psi(\mathbf{x}_i) | \psi(\mathbf{x}_j) \rangle|^2$  which may be used as an estimate for the kernel matrix corresponding to datapoints  $\mathbf{x}_i$  and  $\mathbf{x}_j$ . The main difference between the quantum and classical support vector machines is that in the classical case an explicit kernel function equation is often known, for example the Radial Basis Function (RBF) kernel defined as  $K(\mathbf{x}_i, \mathbf{x}_j) = \exp\left(\frac{-|\mathbf{x}_i - \mathbf{x}_j|^2}{2\sigma^2}\right)$ , where  $\sigma$  is a free parameter that can be optimised. In the quantum case the kernel matrix is instead calculated using a quantum circuit. The classical and quantum support vector machine approaches are summarised in Figure 2.

The first step of the QSVM is to encode classical data  $\mathbf{x}_i$  into a quantum state  $|\psi(\mathbf{x}_i)\rangle$ . In Havlicek et al [10], the encoding circuit comprises of gates that are parameterised by the classical data. The aim of this encoding circuit  $\mathcal{U}(\mathbf{x})$  is to transform each event, a classical  $n$  dimensional array consisting of the momentum coordinates of each particle, into a  $2^n$  dimensional quantum state. The motivation here is that in this higher dimensional Hilbert space it may be easier to separate signal and background events. The input data can be represented as a vector  $\mathbf{x} \in \mathbb{R}^n$  containing all the momentum variables of the particles considered for an event. This vector is mapped onto a quantum state  $|\psi(\mathbf{x})\rangle$  using  $n$  qubits in the following circuit

$$|\psi(\mathbf{x})\rangle = \mathcal{U}(\mathbf{x}) |0\rangle^{\otimes n} = U(\mathbf{x}) H^{\otimes n} U(\mathbf{x}) H^{\otimes n} |0\rangle^{\otimes n}. \quad (3)$$

An encoding circuit  $\mathcal{U}(\mathbf{x})$  is applied to an initial  $|0\rangle^{\otimes n}$  state.  $H^{\otimes n}$  is a parallel implementation of a Hadamard gate on each of the  $n$  qubits and  $U(\mathbf{x})$  is the  $n$ -qubit encoding operation. Note that the encoding operation  $U(\mathbf{x})$  is applied twice within the full encoding circuit  $\mathcal{U}(\mathbf{x})$ . It is also possible to construct the encoding circuit with only one layer, in which case  $\mathcal{U}(\mathbf{x}) = U(\mathbf{x}) H^{\otimes n}$ , or more than two layers.

The encoding operation  $U(\mathbf{x})$  is illustrated in Figure 4. It is formally defined as

$$U(\mathbf{x}) = \exp\left(i \sum_{k=1}^n x_k Z_k + i \sum_{l=1}^{n-1} \sum_{m>l}^n f(x_l, x_m) Z_l Z_m\right), \quad (4)$$

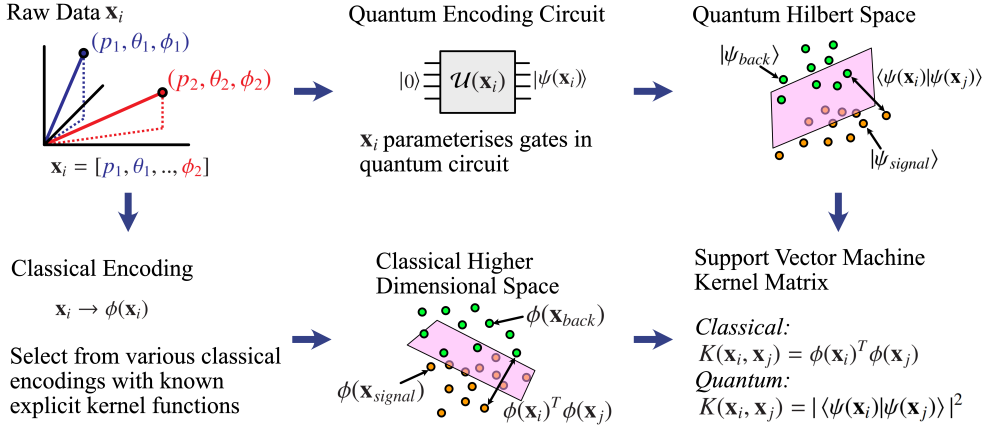


**Fig. 2** (Lower Path) The concept of a classical SVM. Data is encoded in a higher dimensional space where the separation is performed. The inner products between datapoints forms the kernel matrix; this can usually be given as an explicit equation. (Upper Path) The concept of a QSVM. Raw data is encoded into a quantum state using a quantum circuit that is parameterised by the classical data. The separation is made between signal and background in the higher dimensional quantum space. In order to achieve this we need to measure the inner product between the quantum states produced in the circuit.

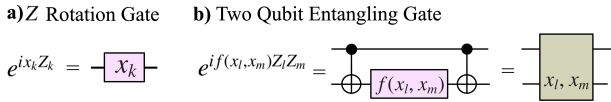


**Fig. 3** **a)** The circuit notation for the single qubit part of the encoding gate. The effect of this Z rotation gate is a Z rotation of the qubit's bloch sphere by an angle  $x_k$ . **b)** The circuit notation we use for the two qubit entangling part of the encoding gate. The explicit construction in a real quantum circuit is shown here using Controlled Not gates. This gate effectively introduces some form of phase shift between two qubits that depends on some function of the respective momentum variables in the classical data  $x_l$  and  $x_m$ .

where  $Z_k$  represents the Pauli Z matrix applied to qubit  $k$ . This circuit introduces a phase shift to each individual qubit by an amount  $x_k$ . The function  $f$  effectively quantifies some form of a phase shift between the two qubits that are to be entangled. The default form of this function is defined as

$$f(x_l, x_m) = (x_l - \pi)(x_m - \pi). \quad (5)$$

This circuit explicitly entangles every qubit with every other qubit, meaning all combinations of qubits are entangled. We will therefore refer to this gate throughout this paper as the combinatorial encoding gate [10].

The purpose of the encoding operation is to turn classical data into a quantum state. In order to use a support vector machine we need to calculate the inner product between every event in this quantum space  $\langle\psi(\mathbf{x}_i)|\psi(\mathbf{x}_j)\rangle$ . By referring to equation (3) this quantity can be written as

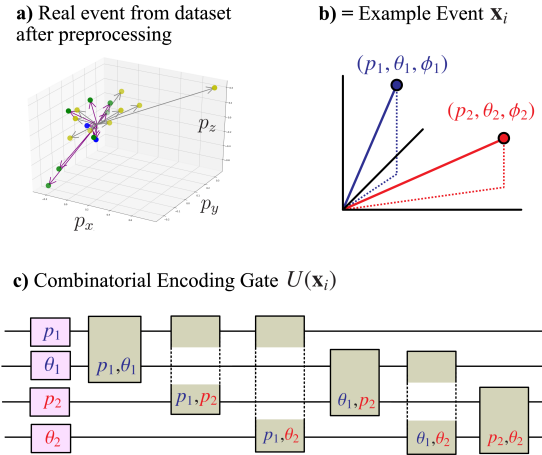


**Fig. 4** **a)** An event from the real dataset after preprocessing is shown. Different coloured points correspond to different types of charged particles. **b)** An example particle decay event containing two particles demonstrating the raw momentum data in spherical coordinates. **c)** The circuit structure for the combinatorial encoding operation  $U(\mathbf{x})$  [10]. For readability the circuit omits the  $\phi$  variable.

$$\langle\psi(\mathbf{x}_i)|\psi(\mathbf{x}_j)\rangle = \langle 0 | H^{\otimes n} U^\dagger(\mathbf{x}_i) H^{\otimes n} U^\dagger(\mathbf{x}_i) U(\mathbf{x}_j) H^{\otimes n} U(\mathbf{x}_j) H^{\otimes n} | 0 \rangle. \quad (6)$$

This kernel estimation circuit, which is illustrated in Figure 5, acts to determine the inner product between the two quantum states. The circuit is run repeatedly over many shots (identical runs) and the proportion of  $|0\rangle^n$  state measurements is calculated. The proportion

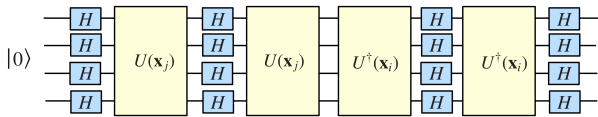


**Fig. 5** The general circuit for estimating the inner product of two quantum encoded states. The probability of measuring  $|0\rangle^n$  as the final state of this circuit will estimate the quantity  $|\langle\psi(\mathbf{x}_i)|\psi(\mathbf{x}_j)\rangle|^2$ .

of  $|0\rangle^n$  measurements is an estimate for the probability  $|\langle 0|H^{\otimes n}U^\dagger(\mathbf{x}_i)H^{\otimes n}U^\dagger(\mathbf{x}_i)U(\mathbf{x}_j)H^{\otimes n}U(\mathbf{x}_j)H^{\otimes n}|0\rangle|^2$ . This process therefore produces an estimate for the quantity  $|\langle\psi(\mathbf{x}_i)|\psi(\mathbf{x}_j)\rangle|^2$  which can then be used as the kernel matrix entry for two events  $\mathbf{x}_i$  and  $\mathbf{x}_j$ . This is repeated for all combinations of events in the dataset until a full kernel matrix is obtained. This kernel is then passed to a classical support vector machine to perform the classification. The overall effect of this is to take events of dimension  $n$  and project them into a  $2^n$  dimensional quantum space where the separation is then performed.

#### 4 Alternative Encoding Gates

The combinatorial encoding gate that is shown in Figure 4 corresponds to a specific kernel. By making adjustments to this encoding circuit we are able to construct entirely different kernels, which have the potential to perform better on our dataset while also using fewer gates and qubits.

##### 4.1 Bloch Sphere Encoding

In an effort to encode the same amount of classical information into fewer qubits we implemented a model that encodes the  $\theta$  and  $p$  variables of each particle into a single qubit. There are several ways in which multiple classical variables can be encoded into a single qubit [14]. To test this concept we construct a circuit that applies an  $X$  rotation by  $\theta$ , followed by a  $Z$  rotation by  $p$  to the bloch sphere of the qubit. This encodes the two variables into the bloch sphere of a single qubit as shown in Figure 6. Note that this circuit contains no quantum entanglement.

##### 4.2 Separate Particle Encoding

The structure of the encoding circuit directly affects the kernel function and the final classification result. One possible issue with the combinatorial encoding circuit is that it treats every classical variable identically;  $p_1$

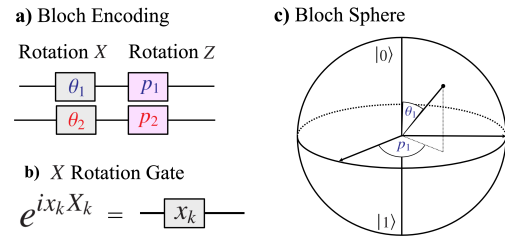


**Fig. 6** a) An encoding circuit that encodes two variables of a particle into a single qubit. b) The definition of the  $X$  rotation gate.  $X_k$  is the Pauli  $X$  matrix applied to qubit  $k$ . c) The resulting bloch spheres of the two qubits, if both initially in the  $|0\rangle$  state, after being acted on by this circuit.

would be entangled with  $\theta_1$  in the same manner as  $p_1$  is entangled with  $p_2$ , despite  $p_2$  being a variable from a different particle. The circuit has no built-in way of discriminating the individual particles. Considering this we introduce a separate particle encoding circuit. The first layer involves entangling the momentum variables for each particle individually, resulting in a 2 qubit quantum state for each particle. This is followed by a layer that entangles the states representing each particle with every other particle based on their momenta.

We can also merge the bloch sphere encoding idea suggested in the previous sub-section into this circuit, by encoding both angles  $\theta$  and  $\phi$  into the same qubit. This allows us to encode three momentum variables into two qubits. This separate particle encoding gate  $U(\mathbf{x})$  is shown in Figure 7 for the 2 particle case. Note that in this circuit the  $\theta$  and  $\phi$  angles of each particle are encoded into the  $\theta$  and  $\phi$  angles of an individual qubit. In this case the encoding function  $f$  has three inputs instead of the usual two; for this we use the following function

$$f(p_1, \theta_1, \phi_1) = (\pi - p_1)(\pi - \theta_1)(\pi - \phi_1). \quad (7)$$

This technique has the advantage of using fewer quantum gates in total, which reduces the error rate when running on a quantum device. It could also be adapted to include additional information about each particle, by expanding the number of qubits to include variables such as charge, mass etc. without as significant an increase in the number of gates used compared to the combinatorial encoding circuit.

## 5 Result Comparisons

The encoding gates discussed here could be used for any number of particles, we have limited our simulations to events that contain exactly 4 particles. The simulations were run with 60,000 training events and 10,000 testing

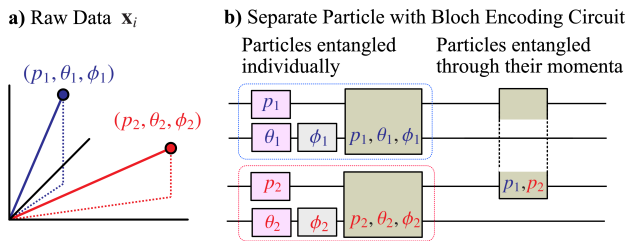


**Fig. 7** a) The raw data classical input for a two particle event. b) The separate particle encoding gate  $U(\mathbf{x})$ . Initially a 2 qubit entangled state is produced for each particle based on each particle’s momentum variables. After individual particle are separately encoded, each particle is then entangled with every other particle through one of its qubits. We also combine the previous bloch sphere encoding from the previous subsection. This results in the  $\theta, \phi$  variables of the particle, being encoded into the  $\theta_b, \phi_b$  of a single qubit’s bloch sphere.

**Table 1** Results obtained by classically simulating various encoding circuits using Qiskit *statevector\_simulator* with 60,000 training events and 10,000 testing events.

Encoding Circuit	Accuracy	AUC
Combinatorial Encoding	0.765	0.827
Separate Particle (Without $\phi$ Bloch)	0.787	0.853
Bloch Sphere Encoding	0.786	0.861
Separate Particle (with Bloch)	0.808	0.877
Classical RBF Kernel SVM	0.794	0.865
XGBoost	0.617	0.648

events using the Qiskit *statevector\_simulator* in the absence of noise [1]. The results of the different encoding circuits mentioned previously are summarised in Table 1.

These results suggest that the physically motivated improvements made in the separate particle circuit have a positive impact on the discriminatory power of the circuit compared to the combinatorial encoding. Furthermore, combining this method with the bloch sphere encoding resulted in our best AUC score of 0.877. For comparison we tested classical SVMs on the data for various kernels with the best result being the RBF Kernel. We also included XGBoost as a comparison, deciding on the hyperparameters (maximum tree depth, number of estimator, minimum split loss and learning rate) using GridSearchCV [20].

## 6 Simulations with Noise and Error Mitigation

The simulation results demonstrate the potential for quantum algorithms on ideal noiseless devices. Modern quantum devices do however have noticeable error rates which are dependent on factors such as the number of gates used in the circuit. To investigate the effect this has on our results we re-run our simulation with a

noise model [1]. In order to reduce the impact of these errors we implement a measurement error mitigation technique [7] recently demonstrated in the context of verifying whole-array entanglement in the IBM Quantum *ibmq\_manhattan* device [18]. This procedure consists of performing a calibration of the basis states for the simulated noisy device at the start. The noisy basis state measurements are used to construct a matrix; the inverse of this matrix when applied to a noisy basis state should take it to the ideal basis state. By applying this calibration matrix to our final results we can reconstruct a final measurement closer to the ideal noiseless case.

The separate particle with bloch encoding circuit was tested using 3 particle events only. The Qiskit *qasm\_simulator* is used with a simulated noise model based on the IBM Quantum *ibmq\_toronto* device. The classification was repeated with 10 different datasets, each consisting of 30 training and 30 testing points to find an average classification performance. The separate particle with bloch encoding circuit achieved an average accuracy of  $0.670 \pm 0.100$  and an average AUC of  $0.751 \pm 0.100$ . For comparison, this test repeated with an ideal noiseless simulation gives an accuracy of  $0.750 \pm 0.050$  and an AUC of  $0.789 \pm 0.110$ .

The introduction of noise does lead to a decrease in the average AUC score for the separate particle encoding circuit from 0.789 to 0.751. In contrast, repeating this investigation for the combinatorial encoding circuit results in an average accuracy of  $0.530 \pm 0.086$  and an average AUC of  $0.550 \pm 0.131$ , a significant reduction in performance in the presence of noise. This could possibly be due to the greater number of gates used in the combinatorial encoding circuit compared to the separate particle with bloch encoding circuit, resulting in a larger source of quantum error.

## 7 Experimental Testing on Real Quantum Devices

The separate particle with bloch encoding circuit was tested on a real device using 3 particle events only. The dataset consisted of 30 training points and 30 testing points. This was run using 6 qubits on the IBM Quantum *ibmq\_casablanca* device and repeated 10 times for the same dataset achieving an average accuracy of  $0.640 \pm 0.036$  and an average AUC of  $0.703 \pm 0.063$ , where the quoted uncertainties in this case are the standard deviation of multiple runs using the same dataset.

The difference in performance between this result and the simulation results in section 5 is linked to the reduced dataset size and inherent errors of real quantum devices. Table 2 shows the comparison of ideal



**Table 2** Results obtained using the separate particle encoding circuit as the training dataset size is varied. The testing dataset size was fixed at 30. Simulations were run using Qiskit then repeated and averaged over 10 different datasets. The Simulated Noise result includes a classical simulation of the noise found in the IBM Quantum *ibmq.toronto* device. The Real Device result refers to a single dataset being run on the IBM Quantum *ibmq.casablanca* device.

Device Type	Training	Accuracy	AUC
Ideal Simulation	1000	$0.77 \pm 0.03$	$0.83 \pm 0.05$
Ideal Simulation	100	$0.75 \pm 0.05$	$0.78 \pm 0.04$
Ideal Simulation	30	$0.75 \pm 0.05$	$0.79 \pm 0.11$
Simulated Noise	30	$0.67 \pm 0.10$	$0.75 \pm 0.10$
Real Device	30	0.64	0.70

simulations of varying training dataset sizes alongside a simulated noise model of the IBM Quantum *ibmq.toronto* device. These results are averaged over 10 random datasets. The uncertainties quoted are the standard deviation of the distribution of trials. The result for the real device was a single run and is consistent within uncertainty of the simulated noise runs.

The trend demonstrates that smaller training datasets result in worse AUC scores. There is then a further drop in performance when quantum noise is taken into account. As the availability and error rates of quantum machines improves over the coming years this opens up the possibility of running larger datasets on less noisy machines and achieving the higher AUC scores reported in Section 5 using simulations.

## 8 Conclusion

We have demonstrated on a small scale how quantum machine learning may be applied to signal-background classification for continuum suppression in the study of B mesons. Simulating the combinatorial encoding circuit on the signal-background classification problem we measured an AUC of 0.827. The separate particle encoding circuit designed for particle data improved the AUC to 0.877, outperforming the classical SVM and XGBoost for this dataset. The separate particle encoding circuit also uses fewer qubits and quantum gates than the combinatorial circuit. Using a smaller dataset in the presence of simulated quantum noise there was a reduction in classification performance for the separate particle encoding method which achieved an average AUC of 0.750, this is attributed to the smaller sample size used and quantum noise. In contrast, the combinatorial circuit in this same set-up performed significantly worse in the presence of simulated noise with an AUC of 0.550, a possible explanation of this could

be the much higher number of gates in the combinatorial circuit compared to the separate particle encoding circuit. Running the separate particle encoding circuit on a real quantum device resulted in an AUC score of 0.703. Further work could involve using quantum error mitigation techniques [6] to improve the performance on real quantum devices in the presence of noise.

When using a limited number of inputs the QSVM outperformed classical methods in simulations. This result suggests that the quantum kernel created by the circuit is, in certain situations, useful for signal background classification. We demonstrate a separate particle encoding circuit that performed best in our noiseless simulations and performed significantly better than the combinatorial circuit in the presence of simulated noise. The number of input data sets and performance in the quantum approach was limited due to the size and error rates of current quantum computers. If expanded to use more data inputs and larger dataset sizes, it is foreseeable that the QSVM may be able to compete with current state-of-the-art classical techniques, which can achieve AUCs of 0.930 [11]. There are also a plethora of alternatives to using an SVM method; quantum generated features created from the encoding gates explored here could be passed to another classical or quantum classifying algorithm. Whether the same encoding circuits that performed well for the QSVM also succeed in other approaches would be a question for further investigation.

**Acknowledgements** This work was supported by the University of Melbourne through the establishment of an IBM Quantum Network Hub at the University. This research was supported by the Australian Research Council from grants DP180102629 and DP210102831. JH acknowledges the support of the Research Training Program Scholarship and the N.D. Goldsworthy Scholarship. CDH is supported by a research grant from the Laby Foundation.

**Conflict of interest** On behalf of all authors, the corresponding author states that there is no conflict of interest.

## References

1. Abraham, H., AduOffei, Agarwal, R., Akhalwaya, I.Y., Aleksandrowicz, G., et al Čepulkovskis: Qiskit: An open-source framework for quantum computing (2019). DOI 10.5281/zenodo.2562110

2. Albertsson, K., Altoe, P., Anderson, D., Anderson, J., Andrews, M., Espinosa, J.P.A., et al: Machine learning in high energy physics community white paper (2019)
3. Arute, F., Arya, K., Babbush, R., et al.: Quantum supremacy using a programmable superconducting processor. *Nature* **574** (2019). DOI <https://doi.org/10.1038/s41586-019-1666-5>. URL <http://dx.doi.org/10.1103/PhysRevA.83.032302>
4. Bapst, F., Bhimji, W., Calafiura, P., Gray, H., Lavrijsen, W., Linder, L.: A pattern recognition algorithm for quantum annealers (2019)
5. Belayneh, D., Carminati, F., Farbin, A., Hooberman, B., Khattak, G., Liu, M., Liu, J., Olivito, D., Pacela, V.B., Pierini, M., Schwing, A., Spiropulu, M., Vallecorsa, S., Vlimant, J.R., Wei, W., Zhang, M.: Calorimetry with deep learning: Particle simulation and reconstruction for collider physics (2019)
6. Endo, S., Benjamin, S.C., Li, Y.: Practical quantum error mitigation for near-future applications. *Phys. Rev. X* **8**, 031027 (2018). DOI 10.1103/PhysRevX.8.031027. URL <https://link.aps.org/doi/10.1103/PhysRevX.8.031027>
7. Qiskit measurement error mitigation. <https://qiskit.org/textbook/ch-quantum-hardware/measurement-error-mitigation.html> (2021). Accessed: 2021-02-12
8. Farhi, E.: Quantum chromodynamics test for jets. *Phys. Rev. Lett.* **39**, 1587–1588 (1977). DOI 10.1103/PhysRevLett.39.1587. URL <https://link.aps.org/doi/10.1103/PhysRevLett.39.1587>
9. Guan, W., Perdue, G., Pesah, A., Schuld, M., Terashi, K., VALLECORSIA, S., vlimant, j.r.: Quantum machine learning in high energy physics. *Machine Learning: Science and Technology* (2020). DOI 10.1088/2632-2153/abc17d. URL <http://dx.doi.org/10.1088/2632-2153/abc17d>
10. Havlicek, V., Córcoles, A.D., Temme, K., Harrow, A.W., Kandala, A., Chow, J.M., Gambetta, J.M.: Supervised learning with quantum enhanced feature spaces (2018)
11. Hawthorne-Gonzalvez, A., Sevier, M.: The use of adversaries for optimal neural network training. *Nuclear Instruments and Methods in Physics Research Section A: Accelerators, Spectrometers, Detectors and Associated Equipment* **913**, 54–64 (2019). DOI <https://doi.org/10.1016/j.nima.2018.10.043>
12. Jeswal, S., Chakraverty, S.: Recent developments and applications in quantum neural network: A review. *Archives of Computational Methods in Engineering* **26** (2018). DOI 10.1007/s11831-018-9269-0
13. Keck, T.: Fastbdt: A speed-optimized and cache-friendly implementation of stochastic gradient-boosted decision trees for multivariate classification (2016)
14. LaRose, R., Coyle, B.: Robust data encodings for quantum classifiers. *Physical Review A* **102**(3) (2020). DOI 10.1103/physreva.102.032420. URL <http://dx.doi.org/10.1103/PhysRevA.102.032420>
15. Lee, S.H., Suzuki, K., Abe, K., Abe, K., Abe, T., Adachi, I., Ahn, B.S., Aihara, H., Akai, K., et al: Evidence for  $B^0 \rightarrow \pi^0 \pi^0$ . *Phys. Rev. Lett.* **91**, 261801 (2003). DOI 10.1103/PhysRevLett.91.261801. URL <https://link.aps.org/doi/10.1103/PhysRevLett.91.261801>
16. Lloyd, S., Schuld, M., Ijaz, A., Izaac, J., Killoran, N.: Quantum embeddings for machine learning (2020)
17. Mooney, G.J., White, G.A.L., Hill, C.D., Hollenberg, L.C.L.: Generation and verification of 27-qubit greenberger-horne-zeilinger states in a superconducting quantum computer (2021)
18. Mooney, G.J., White, G.A.L., Hill, C.D., Hollenberg, L.C.L.: Whole-device entanglement in a 65-qubit superconducting quantum computer (2021)
19. Park, J.E., Quanz, B., Wood, S., Higgins, H., Harishankar, R.: Practical application improvement to quantum svm: theory to practice (2020)
20. Pedregosa, F., Varoquaux, G., Gramfort, A., Michel, V., Thirion, B., Grisel, O., Blondel, M., Prettenhofer, P., Weiss, R., Dubourg, V., Vanderplas, J., Passos, A., Cournapeau, D., Brucher, M., Perrot, M., Duchesnay, E.: Scikit-learn: Machine learning in Python. *Journal of Machine Learning Research* **12**, 2825–2830 (2011)
21. Rebentrost, P., Schuld, M., Wossnig, L., Petruccione, F., Lloyd, S.: Quantum gradient descent and newton’s method for constrained polynomial optimization (2018)
22. Schuld, M.: Quantum machine learning models are kernel methods (2021)
23. Schölkopf, B., A. J. Smola, F., et al, B.: Learning with kernels: support vector machines, regularization, optimization, and beyond (2002)
24. Scikit-learn : Support vector machines. <https://scikit-learn.org/stable/modules/svm.html> (2021). Accessed: 2021-02-12
25. Terashi, K., Kaneda, M., Kishimoto, T., Saito, M., Sawada, R., Tanaka, J.: Event classification with quantum machine learning in high-energy physics. *Computing and Software for Big Science* **5**(1) (2021). DOI 10.1007/s41781-020-00047-7. URL <http://dx.doi.org/10.1007/s41781-020-00047-7>
26. Wu, S.L., Chan, J., Guan, W., Sun, S., Wang, A., Zhou, C., Livny, M., Carminati, F., Meglio, A.D., Li, A.C.Y., Lykken, J., Spentzouris, P., Chen, S.Y.C., Yoo, S., Wei, T.C.: Application of quantum machine learning using the quantum variational classifier method to high energy physics analysis at the lhc on ibm quantum computer simulator and hardware with 10 qubits (2020)
27. Yang, J., Awan, A.J., Vall-Llosera, G.: Support vector machines on noisy intermediate scale quantum computers (2019)
28. Zhong, H.S., Wang, H., Deng, Y.H., Chen, M.C., Peng, L.C., Luo, Y.H., Qin, J.: Quantum computational advantage using photons (2020)